doi:10.26443/seismica.v3i2.1282

SEISMICA

Site characterization of Sikkim Himalaya using HVSR

Mita Uthaman [1], **Chandrani Singh** * [1], **Arun Singh** [1]

[1]Department of Geology and Geophysics, Indian Institute of Technology Kharagpur, Kharagpur, India

Author contributions: *Conceptualization*: Mita Uthaman, Chandrani Singh, Arun Singh. *Validation*: Mita Uthaman, Chandrani Singh, Arun Singh. *Formal Analysis*: Mita Uthaman. *Writing - Original draft*: Mita Uthaman. *Writing - Review & Editing*: Mita Uthaman, Chandrani Singh, Arun Singh. *Visualization*: Mita Uthaman, Chandrani Singh, Arun Singh. *Supervision*: Chandrani Singh, Arun Singh. *Funding acquisition*: Chandrani Singh, Arun Singh.

Production Editor: Carmine Galasso
Handling Editor: Carmine Galasso
Copy & Layout Editor: Miguel Neves

Received: 29 February 2024
Accepted: 2 October 2024
Published: 20 November 2024

Abstract The state of Sikkim in northeast India, located in the central segment of the Himalayan orogen, was plagued by the recent 2011 $\mathrm{M_w}$ 6.9 earthquake. Study of local earthquakes recorded at the network of 27 broadband seismic stations in Sikkim Himalaya unveiled seismogenic zones extending down to lower crustal depths with a predominant strike-slip faulting mechanism. Persistent seismic activity in a region with a complex tectonic setting makes it imperative to study site characteristics crucial for determining the local site conditions. Here, we harness the noise and local earthquakes recorded at the Sikkim network to compute horizontal-to-vertical spectral ratio (HVSR) for site characterization. Comprehensively, local geology and topography are observed to incite distinctly intricate trends in the HVSR curves. The thick sedimentary deposit of the Himalayan foreland basin causes high amplification ($\sim$7) at low resonant frequencies ($<$1 Hz). HVSR curves in the western section of Main Central Thrust Zone exhibit distinct double amplification peaks ($\sim$2.5 at 1 Hz and 5 Hz) possibly due to the parallely dipping sheets of the duplex structure. Whereas, the eastern section of Main Central Thrust Zone exhibits a rather unclear trend owing to its proximity to the transitioning lithological unit. The central section prone to landslides has characteristic peaks at 2 Hz and 8 Hz, possibly indicating the contrasting composition of the sliding surfaces. Collective effects of towering topography and high wind speed are observed to result in anomalously high amplification ($\sim$25) at low frequencies ($<$1 Hz) in north Sikkim. Directional amplification along discrete azimuth signifies the pronounced effect of topography and geometry of lithotectonic units in site response. In conclusion, locally varying site response with prevalent seismicity amplifies the seismic hazard risk potential of Sikkim Himalaya. In particular, central Sikkim is prone to high seismic hazard potential owing to severe seismic hazard level, higher landslide susceptibility, crustal seismicity and high peak amplification.

1 Introduction

Local geology, geomorphology and topography have a strong control over the characteristic seismic motion of a site resulting during incident energy of earthquake signals. The degree of amplification, duration of seismic shaking and its resonant frequency are highly dependent on the local site conditions (Reiter, 1990; Aki and Richards, 2002; Souriau et al., 2007; Bonnefoy-Claudet et al., 2009; Pilz et al., 2009; Gosar et al., 2009). For orogenic regions having a highly complex structural and geological composition, active tectonic and seismic activity, the interplay of these parameters tends to incite complicated response during seismic events. Estimation of local site characteristics in such regions is thus crucial for seismic hazard assessment and territorial urban planning.

Horizontal-to-vertical spectral ratio (HVSR) is a well established non-invasive method for determination of local site characteristics such as peak amplification and its corresponding resonant frequency (Nakamura, 1989). Since orogenic regions do not have a simple 1D layered structure, HVSR curves of earthquakes and microtremors are computed along with that of noise to distinguish and identify the effects of topography and faults (Singh et al., 2019; Yassminh et al., 2019; Rigo et al., 2021). Earthquake HVSRs often deviate from noise HVSR trends due to the wavefield composition of earthquake signal, ground motion strength, and amplification dependent on frequency (Molnar et al., 2022). HVSR of earthquake signals can thus be effectively harnessed to determine the 1D structure vertically below the seismic station (Kawase et al., 2011; Rong et al., 2020). A comprehensive study of earthquake and noise HVSRs can thus aid in deciphering the site characteristics of orogenic regions with complex structure.

A dense network of 27 broadband seismic stations was deployed in April 2019 (Uthaman et al., 2021) to monitor the persistent seismic activity and to decipher the lithospheric architecture of Sikkim Himalaya (Fig. 1). Ambient noise analysis for data validation at the 27 sites revealed the stations stabilized soon after installation and the heterogeneity of the region induced spatially and temporally varying trends (Uthaman et al., 2022). Analysis of data from this network aided in determining the spatially varying seismicity (Uthaman et al., 2023c) with peculiar faulting mechanisms (Uthaman et al., 2023b) arising in a structurally complex crust (Singh et al., 2023; Uthaman et al., 2023a). With spatial variations observed in both noise and seismicity trends, it is imperative to determine the response of the site to incident energy and unravel its cause. In this study, we determine the local characteristics of 27 sites in Sikkim

*Corresponding author: chandrani.gg@iitkgp.ac.in

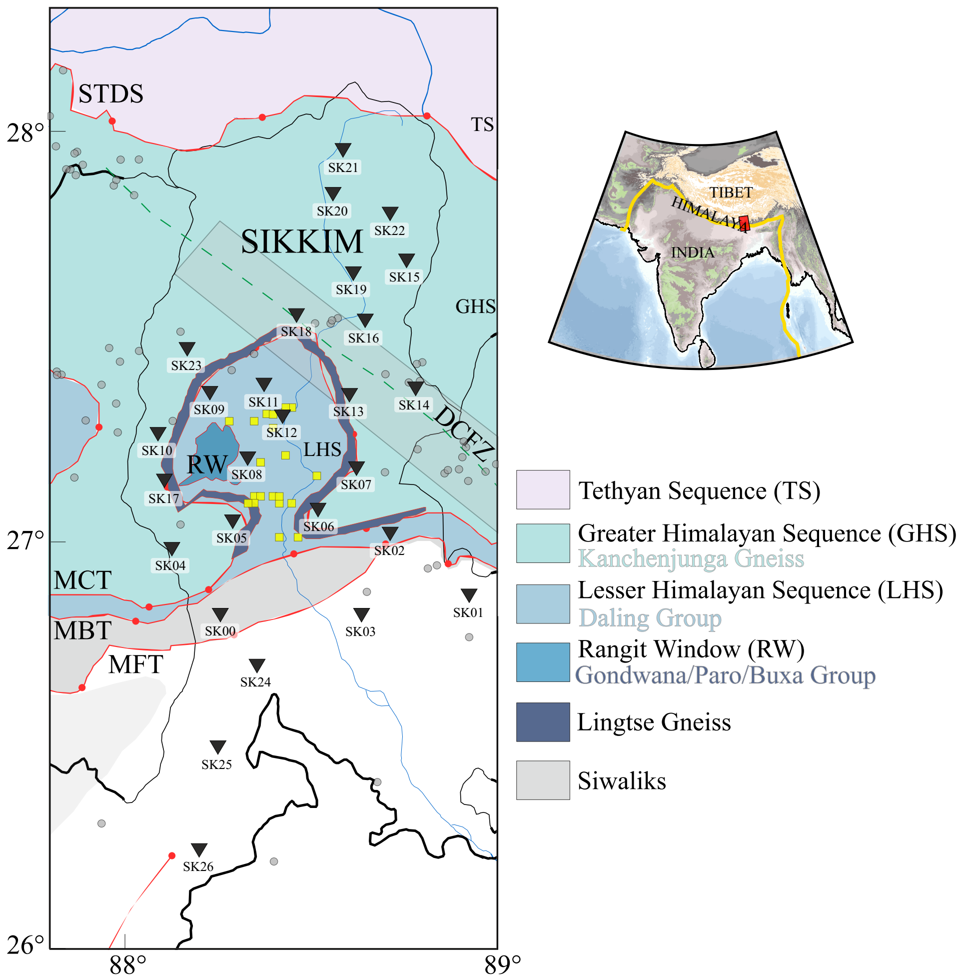

Figure 1 Sikkim seismic network plotted over the geological map of Sikkim Himalaya. Inverted black triangles represent the seismic stations. Grey filled circles are epicentres of local earthquakes ($>M_w$ 2.8). Yellow filled squares represent the locations of landslides that occurred in the region. Legend describes the major lithotectonic units and the corresponding rock type group found in Sikkim Himalaya. Dextrally deforming Dhubri-Chungthang Fault Zone (DCFZ) is highlighted by grey filled rectangle. Major thrust faults are illustrated by red lines. MCT: Main Central Thrust; MBT: Main Boundary Thrust; MFT: Main Frontal Thrust; STDS: South Tibetan Detachment System; RW: Rangit Window. Inset: Map of India with study region highlighted in red.

Himalaya and its adjoining foreland basin to understand the local site effects in such a heterogeneous and complex region. We have used the classical approach of Nakamura (1989) to determine the HVSR curves of ambient noise and local earthquake records. Results indicate local site response to be highly influenced by the local geology and topography, indicating a very complex and heterogeneous seismic hazard scenario.

2 Tectonic and geological setting

The Himalayan orogen serves as a natural laboratory to study the on-going evolution in an active continent-continent collision zone with highly complicated structural and geological composition. Sikkim Himalaya lying in the central part of the orogen has a regionally varying geological composition separated by major thrust faults illustrated in Fig. 1. Region to the south of the Main Frontal Thrust (MFT) is the Himalayan foreland basin composed of thick sedimentary deposits brought down by the Teesta river (Wesnousky et al., 1999). The Main Boundary Thrust (MBT) and MFT bound the fluvial deposits of the Siwalik Group (Gautam and Rösler, 1999). Straddled between the MBT and the overturned Main Central Thrust (MCT), lined by Lingtse Gneiss (Bhattacharyya et al., 2015), is the metasedimentary rocks of the Lesser Himalayan Sequence (LHS) composed of Daling Group (Paul et al., 1996). Nested in the western curve of MCT is the Lesser Himalayan Duplex (LHD) inside the Rangit Window (RW), formed of parallelly dipping thrust sheets (Bhattacharyya and Mitra, 2009). To the north, the Kanchenjunga Gneiss predominant Greater Himalayan Sequence (GHS) is bounded by the MCT and the South Tibetan Detachment System (STDS) (Dasgupta et al., 2009; Bhattacharyya et al., 2015). Striking structural and geological variation across a span of ∼200 km, with equally varying topography coupled with persistent seismicity amplifies the seismic hazard risk potential of the region. The present study of local site characterization attempts at determining the seismic hazard potential of Sikkim Himalaya.

3 Data and Methods

We have used data recorded at the 27 seismic stations in Sikkim Himalaya (Fig. 1). The network consisted of a combination of 3-component Trillium 120P/Q, Trillium Horizon and Trillium Compact broadband sensors which were equipped with Centaur digitizers. All the instruments were procured from Nanometrics Inc. While the Trillium Horizon sensors were buried, Trillium 120P/Q and Trillium Compact were installed on a pier. The different format of installation had minimal interference of ambient noise (Uthaman et al., 2022). The digitizers recorded data in continuous mode at a sampling rate of 50 samples per second from April 2019 to May 2023. The sampling rate is adequate for analysis of HVSR (Wathelet et al., 2020). The dense spatial coverage of the network aids in site characterization of closely located sites thus increasing the resolution of obtained results. We have used Geopsy software (Wathelet et al., 2020) to calculate the horizontal-to-vertical spectral ratio (HVSR) for determination of site characteristics. We used records of both ambient noise and local earthquakes to characterize the local site response. As the region is observed to have a temporal variability of ambient noise (Uthaman et al., 2022), care has been taken by using data recorded during summer months to avoid extreme influence of thermo-barometric variations.

3.1 Analysis of noise

Since our network was operational during the restrictions imposed due to the COVID-19 pandemic, we had a record of signals with least interference from the otherwise persistent anthropogenic noise (Uthaman et al., 2022). We have thus analysed the night-time data (7:00pm – 9:00pm [GMT] which corresponds to 12:30am – 2:30am [IST]) from 20 March 2020 to 10 May 2020, coinciding with the time period during which the restrictions of lockdown were imposed. Though the network stabilized soon after installation (Uthaman et al., 2022), using the data recorded almost a year after installation takes into account the longer duration often required for broadband seismometers to stabilize post deployment (Acerra et al., 2004). This ensured the analysis of the most stationary part of the signal which is essential to extract HVSR of background noise as per the Nakamura (1989) method. The 2-hour long raw data was split into window lengths consisting of at least 50 – 60 s with 1% overlap (Fig. 2). A recording duration of >30 mins ensures resolvability of up to 0.2 Hz fundamental frequency (Acerra et al., 2004). An anti-trigger algorithm (Withers et al., 1998) was applied to eliminate interference of any transient signals (short-term average (STA)=1 s, long-term average (LTA)=30 s). Windows with STA/LTA ratio between 0.20 and 2.50 were retained for computation of HVSR. Amplitude spectra within 0.2 – 25 Hz were subjected to a cosine taper followed by Konno-Ohmachi (Konno and Ohmachi, 1998) smoothing of width 40. Investigation of HVSR curves was restricted to the frequency range of 0.2 – 25 Hz, which is adequate for seismic hazard assessment through site characterization. We have additionally computed azimuthal variation of HVSR curves taking into consideration the drastically varying geology and topography of the study area (Uthaman et al., 2022). HVSR curves were generated in a horizontal plane as a function of azimuth in the range of 0° – 180° by increasing the angle in steps of 10°.

3.2 Analysis of earthquake signals

We also analysed signals of 28 local earthquakes (>M_w 2.8) recorded at the network (Fig. 1) (Uthaman et al., 2023c) to determine the response of the site to incident energy. Part of the signal after S-phase arrival was selected by windows of at least 10 s length for analysis (Fig. 3). This aids in selecting the window with high amplitude of S-wave energy (Singh et al., 2019). Inclusion of signal after S-wave arrival and the corresponding longer time window ensures stability of HVSR curves (Field and Jacob, 1995; Bonilla et al., 1997). Use of longer time length for computation of stable HVSR curves complies with the recommended guidelines as well (Wathelet et al., 2020). Same set of parameters as described above was used for computation of HVSR of earthquake signals. The anti-triggering algorithm was not used so as to enable the energy spikes due to the incident earthquake to be incorporated in the HVSR computation. This aided in determining the resonant frequencies at which the site responds to during the onset of an earthquake signal. Additionally, we have also computed azimuthal variation of earthquake HVSR curves by employing the method used for noise records as well.

4 Results

HVSR curves are calculated for ambient noise and local earthquakes recorded at the 27 seismic stations. Results demonstrate similarity of HVSR trends among stations located within similar lithotectonic units, as evidenced in the shear wave velocities derived from ambient noise tomography (Uthaman et al., 2023a). The results and corresponding discussions are thus classified broadly as per the geology of the lithotectonic units. In this study, HVSR curves of each ambient noise and earthquake signal are represented by deep blue and deep red curves within the selected frequency range of 0.2 – 25 Hz (Figs 4 – 8). Azimuth of peak amplification is highlighted as shaded ellipses of corresponding colours (Figs 4 – 8).

4.1 Siwaliks and Himalayan foreland basin

Stations SK24, SK25, SK26 were located over the thick sedimentary deposits brought down by Teesta river to the Himalayan foreland basin. HVSR curves of noise and earthquake exhibit high amplification (SK24 ∼8, SK25 and SK26 ∼6) at frequencies <1 Hz (Fig. 4, Table 1). Azimuth of peak amplification is observed to be incident from a wide range of ∼10 – 170 °. As we progress from the foreland basin towards the Himalayan foothills composed of Siwaliks, we observe a second peak amplification prominent at ∼10 Hz. The amplification is observed to be more prominent in stations SK01 and SK03 located in closer proximity to Si-

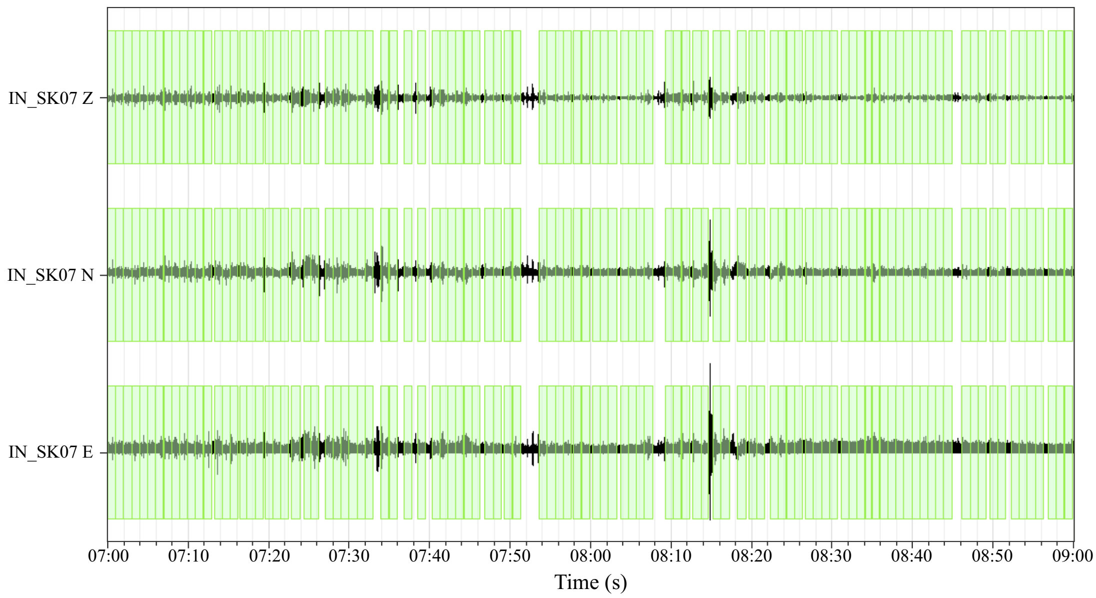

Figure 2 Example waveform of noise recorded in the three components at station SK07 used for analysis. 2-hour long waveform recorded at night-time (7:00pm – 9:00pm [GMT] which corresponds to 12:30am – 2:30am [IST]) is used for analysis. Green rectangles represent selected time windows of at least 50 – 60 s length. Transient signals in the noise record are eliminated by employing the anti-trigger algorithm (Withers et al., 1998).

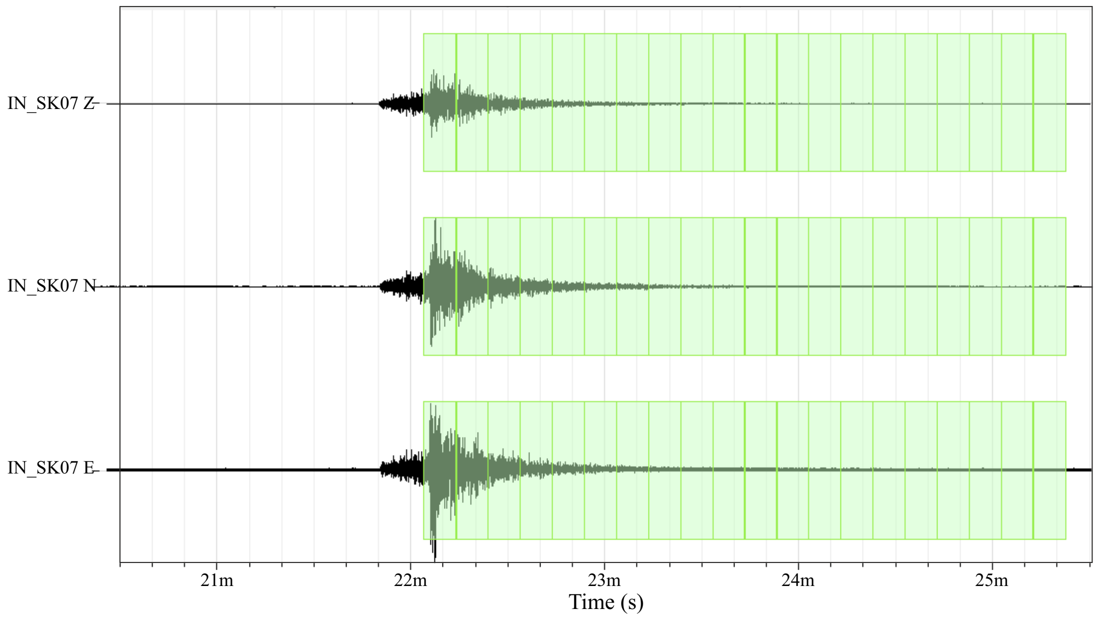

Figure 3 Example waveform of a local earthquake event ($>M_w$ 2.8) recorded in the three components at station SK07 used for analysis. Green rectangles represent time windows of 10 s length selected after S-phase pick.

waliks (Fig. 4, Table 1). Whereas, noise HVSR of station SK00 installed over Siwaliks exhibits an oscillatory trend with amplification less than 2 and no dominant peaks at any fundamental frequency. HVSR of earthquake signals for all the stations located predominantly over sedimentary deposits exhibit a strikingly different trend from HVSR curves of noise. No prominent peak amplification is observed, but rather they exhibit a sinusoidally oscillatory trend.

4.2 Lesser Himalayan Sequence

HVSR curves of noise at stations SK08, SK11 and SK12 located inside the overturned MCT in LHS are observed to have characteristic peak amplifications ($\sim$3) at $\sim$3 Hz and $\sim$7 Hz (Fig. 5, Table 2). Peak amplifications are observed to be incident from azimuths of $\sim$60 – 120° at stations SK08, SK12 and $\sim$10 – 50° at station SK11 (Fig. 5, Table 2). Earthquake HVSRs are observed to mimic the noise HVSRs, except at station SK11 where a higher amplification is prominent. Towards the west, stations SK04, SK05, SK09, SK23 located in proximity of the LHD (Rangit Window) nested in the MCT are observed to have characteristic twin peak amplifications (Fig. 6, Table 2). Both noise and earthquake HVSR has $\sim$2 – 3 amplification corresponding to peaks at $\sim$1 Hz and $\sim$4 Hz (Fig. 5). The first peak has azimuthal direction of $\sim$10 – 60° at the four stations. The second peak is incident from

Station name	f_0 in Hz for noise	A_0 for noise	f_0 in Hz for earthquake	A_0 for earthquake	Azimuth (°)	Nature of peak (as per Acerra et al. (2004))
SK00	unclear	unclear	unclear	unclear	multiple	Unclear peak
SK01	0.4±0.3, 10.86±0.9	1.9±1.75, 3.45±0.94	unclear	unclear	10-170	Two peaks
SK03	0.63±0.39, 11.93±0.48	1.86±0.82, 3.97±0.81	unclear	unclear	10-170	Two peaks
SK24	0.62±0.38	7.58±0.81	NA	NA	10-170	Clear peak
SK25	0.95±0.34	5.46±1.48	NA	NA	10-170	Clear peak
SK26	0.86±0.34	5.72±1.76	unclear	unclear	10-170	Clear peak

Table 1 Average HVSR parameter values at stations installed in the Siwaliks and Himalayan foreland basin

the same azimuth at stations SK04, SK09, SK23, with no prominent azimuthal incidence at SK05. Stations SK04 and SK23 have additional incidence from azimuth of ~120 – 170° (Fig. 6, Table 2). The HVSR curves of earthquake signals in this part of the study region are also observed to mimic the noise HVSRs (Fig. 6, Table 2). On the contrary, as opposed to the clear peaks observed at the aforementioned stations, HVSR curves at stations SK06, SK07 and SK13 do not exhibit any prominent peak amplification (Fig. 7, Table 2). These stations were located at the eastern edge of the overturned MCT above the Lingtse Gneiss (Fig. 1). The obscurity in peak amplification and fundamental resonant frequency is further evident in azimuthal direction as well, with energies observed to be incident from multiple azimuths (Fig. 7, Table 2). Earthquake HVSRs are observed to mimic the noise HVSRs at these stations (Fig. 7, Table 2).

4.3 Higher Himalayan Sequence

Given the ease of accessibility in Sikkim Himalaya unlike the rest of the Himalayas, a significant number of stations were installed at high elevations (Uthaman et al., 2022). HVSR curves at stations SK14, SK15, SK16, SK17, SK18, SK19, SK20, SK22 (Fig. 8, Table 3) and SK23 (Fig. 6, Table 2), are observed to have extreme amplifications of up to ~25 with a broad peak at frequencies <1 Hz. Station SK22 in the northern part of the study region has an exceptional amplification of ~50. Earthquake HVSRs are observed to mimic the noise HVSRs at frequencies superseding 1 Hz. On the contrary, earthquake HVSR of SK20 is observed to not follow the noise HVSR in any frequency range. Furthermore, of the stations located at high elevation, stations SK19 and SK21 exhibit an anomalous HVSR trend (Supplementary Figure 1). SK19 has a rather irregular HVSR trend, whereas SK21 has anomalous peaks at high frequencies (~10 Hz and ~11 Hz). Azimuth of peak amplification at all stations are also highly heterogeneous.

5 Discussion

5.1 Effect of sedimentary deposits

High peak amplification at low frequencies is a characteristic HVSR trend observed for lithology consisting of loose sedimentary deposits overlying the sedimentary basin (Bonnefoy-Claudet et al., 2006, 2009; Pastén et al., 2016). The observed peak amplification at <1 Hz at stations (SK24, SK25, SK26) over the sedimentary basin thus reflects the thick deposit of soft material. The pronounced effect of sedimentary deposits is observed in various studies conducted in this region. Higher ambient noise levels prevalent in horizontal components of the seismometer (Uthaman et al., 2022) located on the thick sedimentary cover of ~10 km (depth constraints placed by receiver function (Singh et al., 2023) and shear wave velocity studies (Uthaman et al., 2023a)) overlying the high density material of Rajmahal Traps (Tiwari et al., 2006; Pavankumar and Manglik, 2021; Uthaman et al., 2023a) corroborate the high peak amplification arising due to the sharp impedance contrast. The thick sediment cover is observed to cause higher scattering of energy due to increased reflection and refraction in the sediments (Shapiro et al., 1998). The amplification incident due to such scattering from a wide range of azimuths (~10 – 170°) could be indicative of energy incident from all directions due to the widespread cover of sedimentary deposits in the region. The decreasing thickness of sedimentary cover towards the foothills of Himalaya (Singh et al., 2023; Uthaman et al., 2023a) is evidenced by increasing HVSR peak at higher frequency (~10 Hz) at stations SK01 and SK03 located over the sedimentary basin, but in proximity to Siwaliks. The result is indicative of decreasing depth to underlying bedrock towards the foothills (La Rocca et al., 2020). This transition is evidenced by decreasing thickness of sedimentary cover towards the foothills (Singh et al., 2023; Uthaman et al., 2023a). The HVSR curve at seismic station SK00 installed over Siwaliks is observed to have multiple unclear peaks incident from varying azimuths. Lack of clear amplification at any fundamental frequency can possibly be resulting from stiff sediments of the Siwaliks lying over bedrock (Acerra et al., 2004). Multiple peaks exhibiting an oscillatory trend in HVSR of earthquake signals at all seismic stations located over sediments indicate anomalous amplification possibly arising due to higher reflection of surface waves in the sediments (Shapiro et al., 1998; Uthaman et al., 2022).

5.2 Structural variations in MCT

LHS bounded by the overturned MCT in Sikkim is composed dominantly of Daling Group (Paul et al., 1996). Regions with lithological unit of Daling Group predominantly consisting of Gorubthan Formation is observed to be more susceptible to landslides (Kaur et al., 2019). East and South Sikkim comprised of this geological composition have thus experienced several landslides (Fig. 1). Landslide prone regions have a characteristic slip surface distinguishing the surrounding con-

Station name	f_0 in Hz for noise	A_0 for noise	f_0 in Hz for earthquake	A_0 for earthquake	Azimuth (°)	Nature of peak (as per Acerra et al. (2004))
SK04	0.88±0.40, 6.05±0.50	2.40±0.87, 2.42±0.79	0.85±0.35, 6.96±0.65	2.48±0.45, 2.56±0.48	120-170	Two peaks
SK05	1.62±0.52, 4.02±0.95	2.76±1.89, 1.97±0.50	1.65±0.66, 3.98±0.49	3.12±0.98, 2.01±0.85	120-170	Two peaks
SK09	0.79±0.31, 4.12±1.11	1.78±0.86, 1.69±0.43	1.00±1.52, 4.25±0.85	2.12±1.56, 1.68±0.52	120-170	Two peaks
SK23	1.01±0.44, 4.22±1.19	2.72±0.69, 2.30±0.78	1.22±0.56, 4.18±0.58	2.55±0.54, 2.38±0.76	120-170	Two peaks
SK08	2.45±0.80, 7.67±0.67	2.21±1.54, 1.50±0.49	2.58±0.91, 7.52±0.45	2.57±1.21, 1.8±0.64	60-120	Two peaks
SK11	2.16±0.87, 6.65±0.82	1.17±0.79, 1.01±0.46	3.25±0.75, 6.70±0.71	4.25±0.68, 1.21±0.52	10-50	Two peaks
SK12	2.75±0.69, 7.62±0.85	2.11±1.03, 2.01±0.46	2.78±0.52, 7.55±0.79	2.51±1.01, 2.32±0.58	10-50	Two peaks
SK02	unclear	unclear	unclear	unclear	unclear	Unclear peaks
SK06	unclear	unclear	unclear	unclear	unclear	Unclear peaks
SK07	unclear	unclear	unclear	unclear	unclear	Unclear peaks
SK13	unclear	unclear	unclear	unclear	unclear	Unclear peaks

Table 2 Average HVSR parameter values at stations installed in the Lesser Himalayan Sequence

Station name	f_0 in Hz for noise	A_0 for noise	f_0 in Hz for earthquake	A_0 for earthquake	Azimuth (°)	Nature of peak (as per Acerra et al. (2004))
SK14	1.09±0.62	10.21±0.50	15.27±1.55	3.34±1.72	60-170	Broad low f_0 peak
SK15	0.85±0.27	3.37±1.14	1.06±0.26	3.68±1.21	10-170	Broad low f_0 peak
SK16	0.77±0.26	8.34±1.12	1.71±0.61	5.01±1.51	10-170	Broad low f_0 peak
SK17	0.71±0.25	3.78±1.91	3.06±0.25	3.47±0.97	10-70	Broad low f_0 peak
SK18	0.73±0.19	5.57±0.47	8.95±0.58	1.64±0.65	60-170	Broad low f_0 peak
SK20	0.79±0.25	5.01±0.97	6.25±0.47	3.67±0.84	10-170	Broad low f_0 peak
SK22	0.75±0.17	50±1.25	5.49±1.32	2.69±0.82	10-120	Broad low f_0 peak
SK19	unclear	unclear	unclear	unclear	multiple	Multiple peaks
SK21	unclear	unclear	unclear	unclear	unclear	Unclear peaks
SK10	unclear	unclear	unclear	unclear	unclear	Unclear peaks

Table 3 Average HVSR parameter values at stations installed in the Higher Himalayan Sequence

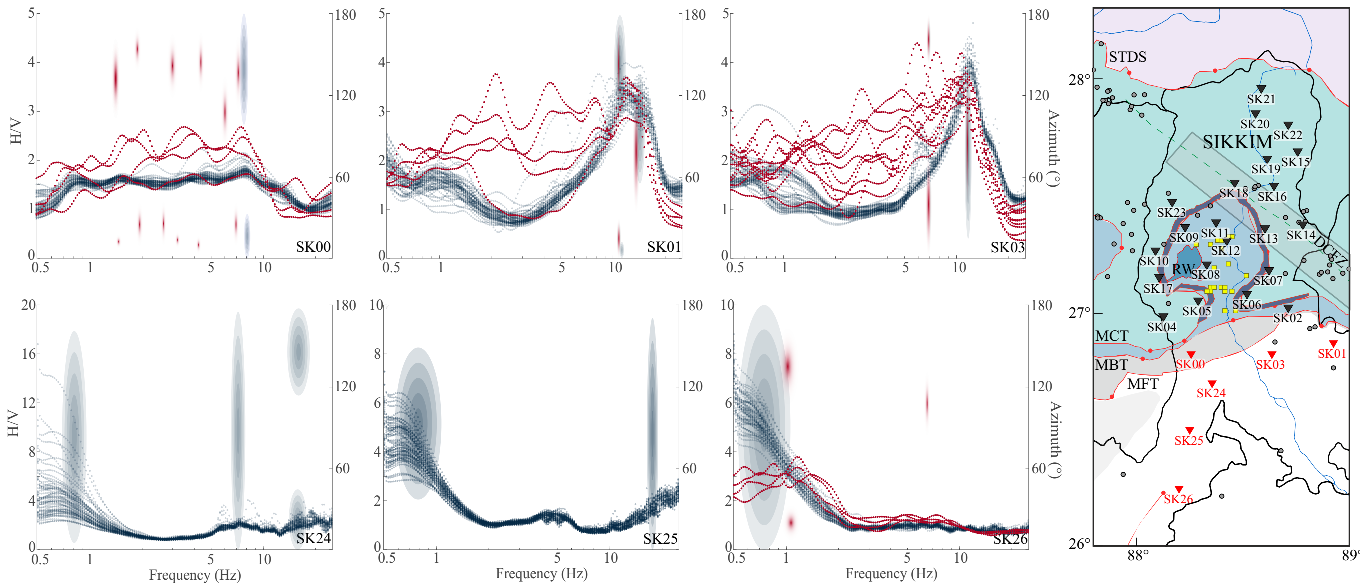

Figure 4 HVSR curves analysed at stations SK00, SK01, SK03, SK24, SK25 and SK26 installed over Siwaliks and Himalayan foreland basin. Blue and red curves are HVSR curves of noise and earthquakes respectively. Blue and red filled ellipses represent predominant azimuths of directional HVSRs. Inset: Geological map of Sikkim Himalaya with red inverted triangles representing seismic stations for which the results are visualized. Rest of the symbols are as described in Fig. 1. MCT: Main Central Thrust; MBT: Main Boundary Thrust; MFT: Main Frontal Thrust; STDS: South Tibetan Detachment System; DCFZ: Dhubri-Chungthang Fault Zone; RW: Rangit Window.

trasting layers (Ávila Barrientos et al., 2023). Signatures of such contrasting layers can be effectively captured by HVSR curves demonstrating multiple peaks at distinct frequencies (Panzera et al., 2012; Galea et al., 2014; Pazzi et al., 2017). Studies show HVSR curves in landslide zones have characteristic peaks at ∼2 Hz and ∼8 Hz (Hussain et al., 2019). In our study, stations SK08, SK11 and SK12 located in South Sikkim over the Daling Group of LHS were located in close proximity to landslide prone regions of Sikkim (Fig. 5). HVSR

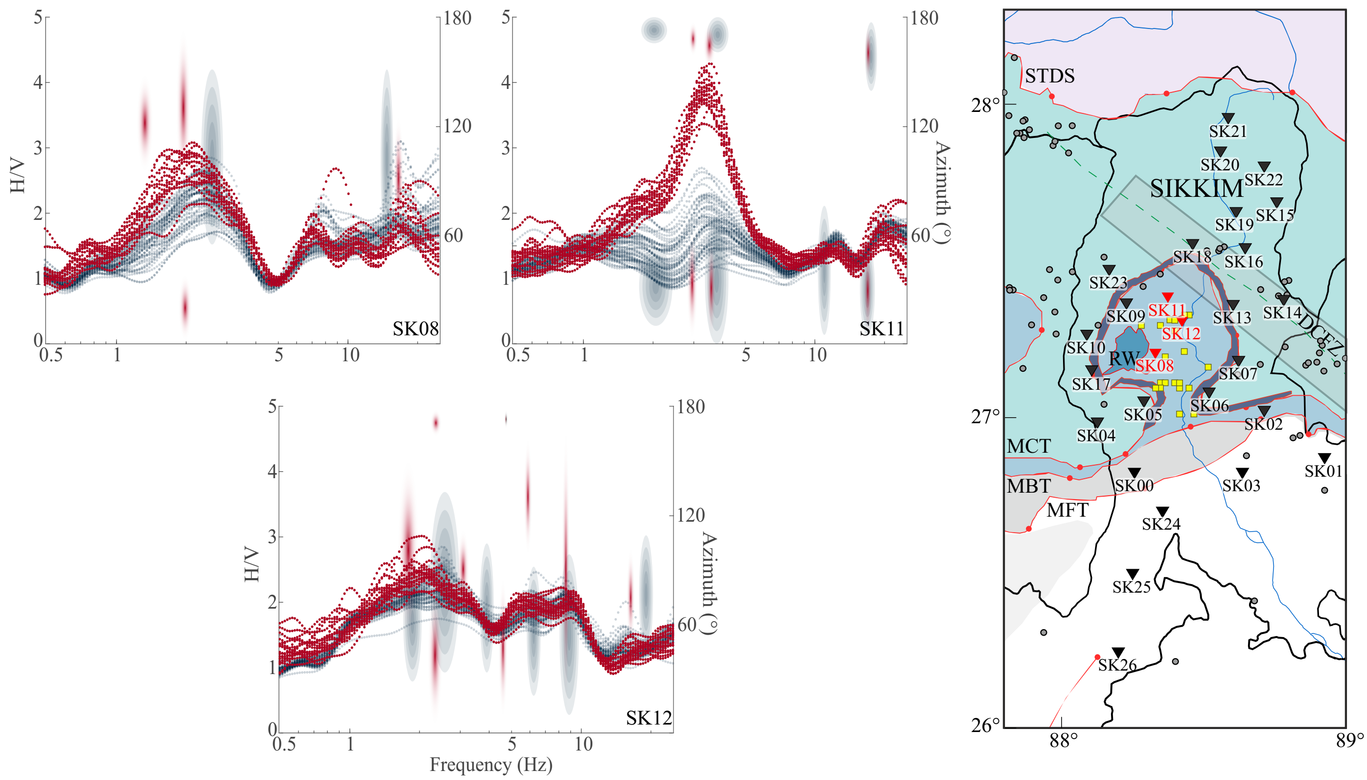

Figure 5 HVSR curves analysed at stations SK08, SK11, and SK12 installed in Main Central Thrust Zone in proximity to landslide prone regions. Blue and red curves are HVSR curves of noise and earthquakes respectively. Blue and red filled ellipses represent predominant azimuths of directional HVSRs. Inset: Geological map of Sikkim Himalaya with red inverted triangles representing seismic stations for which the results are visualized. Rest of the symbols are as described in Fig. 1. MCT: Main Central Thrust; MBT: Main Boundary Thrust; MFT: Main Frontal Thrust; STDS: South Tibetan Detachment System; DCFZ: Dhubri-Chungthang Fault Zone; RW: Rangit Window.

curves at these stations have characteristic peaks at ∼3 Hz and ∼7 Hz possibly indicating contrasting layers around the sliding surface. A predominance of incident energy along ∼60 – 120° azimuth at SK08 and SK12, and ∼10 – 60° at SK11 is observed (Fig. 5). This could be indicative of directional amplification arising due to fractures or cracks present in the sliding-bodies (Bonamassa and Vidale, 1991; Imposa et al., 2016; Alonso-Pandavenes et al., 2023). Directional amplification in landslide prone regions is well-studied (Maresca et al., 2022), though whether the indication of the azimuth is along (Guerriero et al., 2016) or normal (Moore et al., 2011; Burjánek et al., 2019) to the sliding surface is highly debated. Along with the ambiguity in azimuthal HVSR, a distinct amplification of earthquake HVSR is prominent at station SK11 while earthquake and noise HVSRs are observed to mimic each other at station SK08 and SK12 (Fig. 5). Given the factors needed to be considered is vast, delving further into resolving the geometry of landslide prone surface requires a much detailed study. Since this is out of scope for the present study, we have commenced a separate study to characterize the landslide prone zones in Sikkim Himalaya using HVSR (Uthaman et al., 2024a).

Duplex structures in Himalaya are stated to provide efficient mechanism to accommodate thickening arising due to the active thrusting of the orogen (DeCelles and Mitra, 1995). Nested in the western curve of the overturned MCT is the Rangit Window (RW) (Fig. 1) which is the Lesser Himalayan Duplex formed of repeated units of Gondwana, Buxa and Daling Groups creating an antiformal stack (Bhattacharyya et al., 2015). Sites in proximity to such complex geological and structural composition are often observed to exhibit peculiar HVSR trends with two or more peak amplifications at distinct fundamental frequencies (Pazzi et al., 2017). HVSR curves possessing multiple peaks at different frequencies are stated to be arising due to alternating layers of distinct lithology (Lermo and Chávez-García, 1993; Fäh et al., 2001), possibly due to its inclined dipping geometry (Stanko et al., 2017). In our study region, stations SK04, SK05, SK09, and SK23 located in proximity of RW exhibit characteristic twin peak amplifications (Fig. 6). The multiple peaks could well correspond to the impedance contrasts of the parallely dipping stacked thrust sheets with alternating lithological units. Broadened peaks further attest to the presence of dipping resonators (Dietiker et al., 2018; Molnar et al., 2018). As for directional amplification, both peaks have an azimuthal angle of ∼10 – 60°, with SK04 and SK23 having additional energy incident at ∼120 – 170° azimuth (Fig. 6). The directional amplification could be parallel to the dipping direction, resulting from polarization due to reflection, wave trapping or resonance in the parallel layers (Pischiutta et al., 2010; Panzera et al., 2016). The additional azimuthal energy at SK04 and SK23 could be due to the concerned stations' spatial location with respect to the RW. Earthquake HVSRs

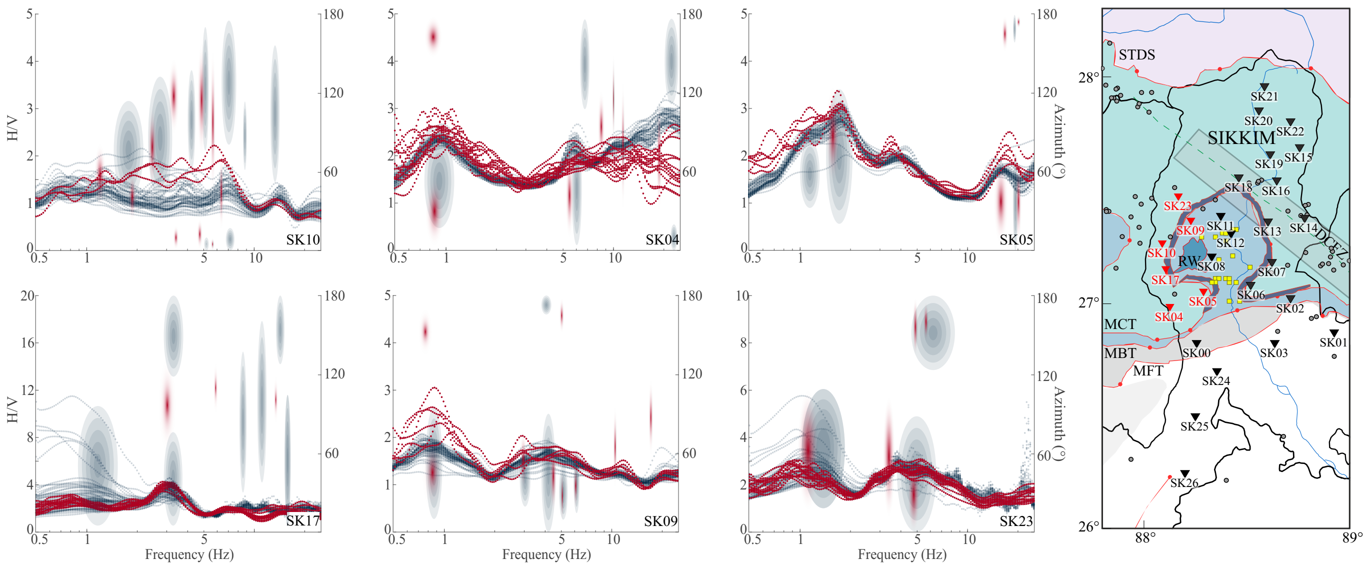

Figure 6 HVSR curves analysed at stations SK04, SK05, SK09, SK10, SK17 and SK23 installed in Main Central Thrust Zone in proximity to the Lesser Himalayan Duplex structure in the Rangit Window. Blue and red curves are HVSR curves of noise and earthquakes respectively. Blue and red filled ellipses represent predominant azimuths of directional HVSRs. Inset: Geological map of Sikkim Himalaya with red inverted triangles representing seismic stations for which the results are visualized. Rest of the symbols are as described in Fig. 1. MCT: Main Central Thrust; MBT: Main Boundary Thrust; MFT: Main Frontal Thrust; STDS: South Tibetan Detachment System; DCFZ: Dhubri-Chungthang Fault Zone; RW: Rangit Window.

mimicking the noise HVSRs indicate amplification of earthquake signals along the dipping layers of the RW. Results of high shear wave velocity and negative radial anisotropy corresponding to the compressional stress prevalent in the complex dipping thrust sheets in RW (Uthaman et al., 2023a) corroborates with our results. As for stations SK10 and SK17 located in proximity to RW, the noise and earthquake HVSRs do not exhibit any trend with multiple peaks (Fig. 6). We refrain from interpreting the HVSR of SK10 as it does not qualify the peak clarity criteria of the SESAME guideline (Acerra et al., 2004). The curve has no peak exceeding amplification of 2, but rather has oscillatory peaks incident from multiple azimuths. The station located at the confluence of valleys over the gneissic formation of GHS could be possibly inciting such a site response (Acerra et al., 2004). Whereas, for station SK17 located at a towering elevation of 2438 m (Uthaman et al., 2022) is likely responsible for the amplification of ~8 at low frequency (~0.75 Hz).

MCT separating the LHS and GHS is lined by lenses of Lingtse Gneiss in Sikkim Himalaya (Bhattacharyya et al., 2015). This marks the transition zone of lithological units. Regions with such transition zones along slopes of the topography are observed to exhibit an irregular trend in HVSR curve, with no prominent amplification corresponding to any fundamental frequency (Stanko et al., 2017). Irregularly shaped peaks with equally irregular azimuthal HVSR trends are often indicative of lateral heterogeneity (Stanko et al., 2017). In our study region, stations SK02, SK06, SK07, and SK13 located along the Lingtse lenses of eastern curve of MCT exhibit a very irregular HVSR trend (Fig. 7). Earthquake HVSR and azimuthal HVSR mimic the irregularity of noise HVSR (Fig. 7). The overall trend is a strong indicator of transitioning lithology along complex topography. As compared to the eastern curve, the irregularity of HVSR trend along western section could possibly have been masked by the prominent effects of the RW giving rise to variation in HVSR trends.

5.3 Effect of topography

GHS composed of high grade crystalline rocks generally has a high topographic relief. The stations located in the GHS were thus situated over mountains with elevation as high as 4000 m (Uthaman et al., 2022). Topography is observed to have a significant effect on site response in many studies (Chávez-García et al., 1996; Burjánek et al., 2014; La Rocca et al., 2020). Anomalous amplification is stated to occur due to ridge crests over topographies having a convex construct (Geli et al., 1988; Del Gaudio et al., 2008; Formisano et al., 2012), and deamplification in the base of hills and valleys resembling a concave topography (Bard and Riepl-Thomas, 2000). It often becomes difficult to deconvolve the site effects produced due to topography and that due to local geology (La Rocca et al., 2020). Coupled with the complex topography on which these stations are located, the wind speeds are significantly high at the towering elevation of the mountains. Higher wind speeds tend to induce noise in the horizontal components which gets reflected in the low frequency range of HVSR curves (Mucciarelli et al., 2005; Bland and Gallant, 2002). The combined effects of topography and wind speed are observed to result in HVSR curves with high amplification at low frequencies (~1 Hz) at stations SK14, SK15, SK16, SK18, SK20, SK22 (Fig. 8) and SK17 (Fig. 6). The higher degree of variability of noise HVSRs at frequency less than 1 Hz could be a possible indication of effect of wind speed. On the contrary, earthquake HVSRs have stable trend at low frequencies and match the noise HVSR otherwise.

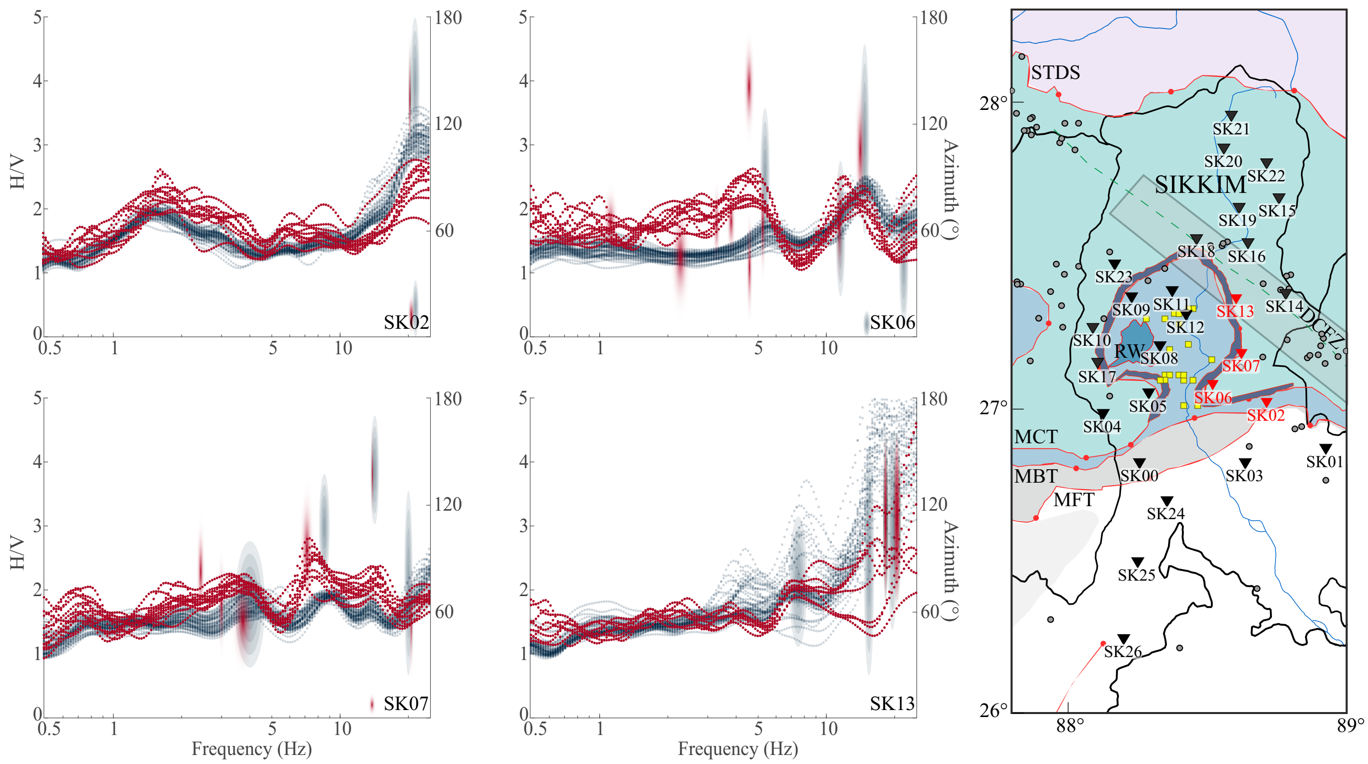

Figure 7 HVSR curves analysed at stations SK02, SK06, SK07 and SK13 installed in Main Central Thrust Zone in proximity to lenses of Lingtse Gneiss. Blue and red curves are HVSR curves of noise and earthquakes respectively. Blue and red filled ellipses represent predominant azimuths of directional HVSRs. Inset: Geological map of Sikkim Himalaya with red inverted triangles representing seismic stations for which the results are visualized. Rest of the symbols are as described in Fig. 1. MCT: Main Central Thrust; MBT: Main Boundary Thrust; MFT: Main Frontal Thrust; STDS: South Tibetan Detachment System; DCFZ: Dhubri-Chungthang Fault Zone; RW: Rangit Window.

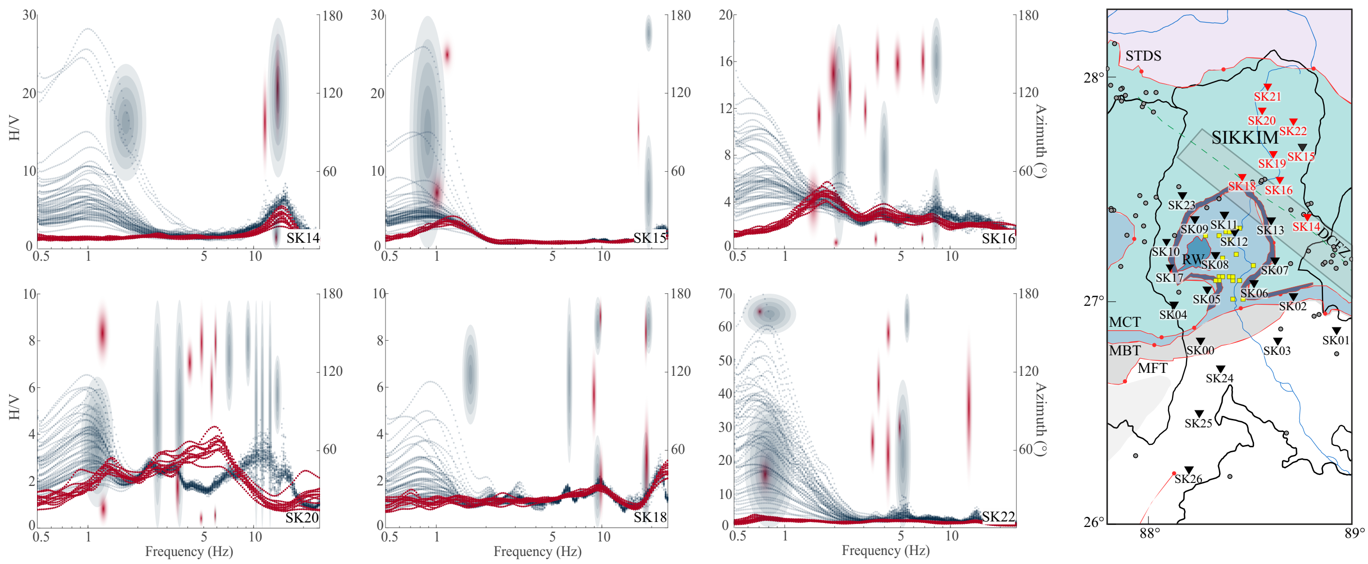

Figure 8 HVSR curves analysed at stations SK14, SK15, SK16, SK18, SK20, and SK22 installed at high elevations in the Greater Himalayan Sequence. Blue and red curves are HVSR curves of noise and earthquakes respectively. Blue and red filled ellipses represent predominant azimuths of directional HVSRs. Inset: Geological map of Sikkim Himalaya with red inverted triangles representing seismic stations for which the results are visualized. Blue filled triangles represent seismic stations at which anomalous HVSR curves are observed. Rest of the symbols are as described in Fig. 1. MCT: Main Central Thrust; MBT: Main Boundary Thrust; MFT: Main Frontal Thrust; STDS: South Tibetan Detachment System; DCFZ: Dhubri-Chungthang Fault Zone; RW: Rangit Window.

Thus, earthquake HVSR exhibiting high amplification at low frequency for stations located over compact geology indicates prominent effect of topography on peak amplification.

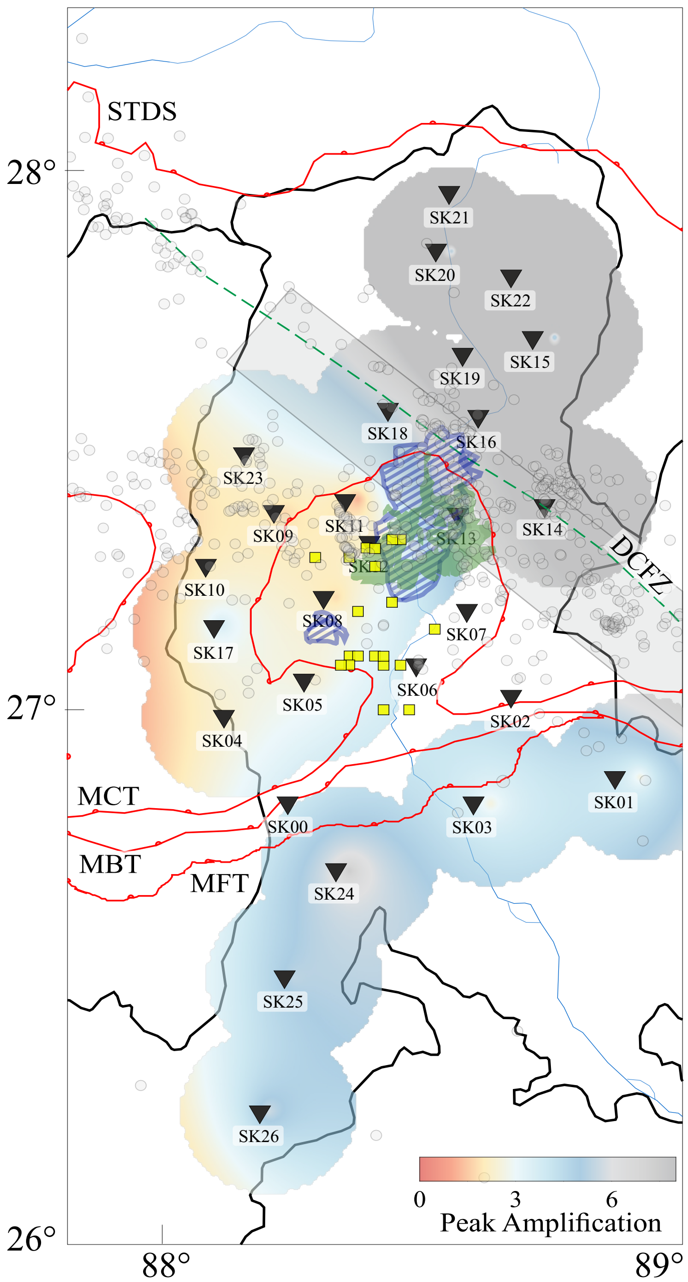

Figure 9 Spatial variation of peak amplification across Sikkim Himalaya. Blue stripped area demarcates region prone to severe hazard level obtained from seismic hazard zonation mapping of Pal et al. (2007). Green filled area indicates region with higher landslide susceptibility coinciding with severe hazard level region, obtained from Sonker et al. (2024). Yellow filled squares represent location of landslides occurred in the region. Open circles are hypocentres of local earthquakes occurred between April 2019 and May 2023 (Uthaman et al., 2024b). Black filled inverted triangles represent seismic stations from the Sikkim network (Uthaman et al., 2021). Dextrally deforming Dhubri-Chungthang Fault Zone (DCFZ) is highlighted by grey filled rectangle. Major thrust faults are illustrated by red lines. MCT: Main Central Thrust; MBT: Main Boundary Thrust; MFT: Main Frontal Thrust; STDS: South Tibetan Detachment System; DCFZ: Dhubri-Chungthang Fault Zone; RW: Rangit Window.

5.4 Seismic hazard assessment of Sikkim Himalaya

Given the spatially varying ambient noise environment (Uthaman et al., 2022) and observed variation in site characteristics across the Sikkim Himalaya, it is crucial to assess the region for potential seismic hazard in the wake of persistent seismicity (Uthaman et al., 2024b). As observed, multiple sites in Sikkim have two characteristic resonant frequencies but within similar range of peak amplification (Tables 1 and 2). We thus interpolate values of peak amplification within a 20 km search radius using nearest neighbour interpolation scheme (Wessel et al., 2019). Spatial interpolation reveals highest peak amplification in the GHS at stations located at high elevation (Fig. 9). As the high amplification is a result of effect of topographic relief coupled with high wind speeds, the underlying high-grade metasedimentary rocks of GHS is less susceptible to seismic hazard. We interpret this region categorized with low seismic hazard level as per Earthquake Hazard Index (Pal et al., 2007) coupled with negligible seismic activity (Uthaman et al., 2024b) to have lower seismic hazard potential. Apart from the GHS, high peak amplification is observed in LHS of central Sikkim Himalaya and the sedimentary basin of northern West Bengal (Fig. 9). Higher amplification is expected to occur in the loose sediments brought down by Teesta river to the Himalayan foreland basin. Despite the absence of active faults and no seismic activity (Uthaman et al., 2024b) in the current scenario, the region could have a high seismic hazard potential owing to high peak amplification. The most intriguing region is central Sikkim in LHS with high peak amplification. The region categorized as severe seismic hazard level (Pal et al., 2007), coincides with landslide prone areas with high landslide susceptibililty (Sonker et al., 2024) and high seismicity (Uthaman et al., 2024b). Seismicity arising along the underlying Main Himalayan Thrust in the upper crust and due to dextrally deforming DCFZ in the mid-crust (Uthaman et al., 2024b) raises the seismic hazard potential and possibility of surface damage from high amplification. Quantification of seismic hazard potential requires additional processing from multiple datasets, due to which we refrain from quantifying the same, but are rather providing qualitative estimates in this study.

6 Conclusions

The structural and geological complexity of the Himalayas resulting from its intricate evolution are well reflected in the site characterization study of the Sikkim Himalaya. The local site response obtained from the noise and earthquake records at the 27 seismic stations reveals a rather complex structure. Interpretation of the peak amplifications and resonant frequencies required consideration of the local geology, topographic relief and meteorological parameters, complicating the rather simple 1D interpretation often followed for HVSR curves. Following are the key findings concluded from the site characterization study in Sikkim Himalaya and its adjoining foreland basin:

- Siwaliks and the Himalayan foreland basin lying adjacent to the Sikkim Himalayas has HVSR trends characteristic to the abundant sedimentary deposits in the region, with high amplifications at low frequencies.
- LHS bounded by MCT is highly affected by distinct local geology. While the western section is affected by the duplex structure, the eastern section shows signatures characteristic to changing lithological units.
- Regions prone to frequent landslides exhibit a typical directional amplification due to the contrasting composition along the sliding surface.
- The high wind speeds of GHS dominate the HVSR trends of noise, while the earthquake HVSRs are more reflective of the high amplification caused by the complex topographic relief of the region.
- Central Sikkim Himalaya can be qualitatively classified as region with high seismic hazard potential owing to severe seismic hazard level, higher landslide susceptibility, crustal seismicity and high peak amplification.

Sikkim Himalaya thus has a very heterogeneous site characteristic majorly influenced by local geology and topography. The conjunction of landslide prone areas in Sikkim to that where shallow earthquakes tend to concentrate (Uthaman et al., 2024b) raises the seismic hazard susceptibility of the region. Neighbouring sites exhibiting a strong dependence of site characteristics on local geology and topography along with a few anomalous HVSR trends complicates the hazard potential mapping.

Acknowledgements

The project is funded by Ministry of Earth Sciences, Government of India, through a research grant (MoES/P.O.(Seismo)/1(318)/2017, SDH). We thank team members A. K. Tiwari, A. K. Dubey, S. Sarkar, N. Jana, A. Dutta and G. Kumar for their efforts in the field during the survey and installation period. The team would like to acknowledge the support and cooperation of the government of Sikkim State (Department of Science and Technology) and the people residing in the project deployment areas. We would also like to extend our thanks to the editor Carmine Galasso, and two anonymous reviewers for their consideration and valuable insights which greatly helped in improving the manuscript.

Data and code availability

Raw data for this research was acquired under third party restrictions imposed by the funding agency (Ministry of Earth Sciences, Govt. of India). Seismic data used in this study is available publicly under India's Scheme for Promotion of Academic and Research Collaboration (SPARC) (https://sparc.iitkgp.ac.in/), and will also be made available on personal collaborative requests.

Competing interests

The authors state no competing interests.

References

Acerra, C., Aguacil, G., Anastasiadis, A., Atakan, K., Azzara, R., Bard, P.-Y., Basili, R., Bertrand, E., Bettig, B., Blarel, F., et al. Guidelines for the implementation of the H/V spectral ratio technique on ambient vibrations measurements, processing and interpretation. *European Commission–EVG1-CT-2000-00026 SESAME*, 2004.

Aki, K. and Richards, P. *Quantitative Seismology*. University Science Books, 2002.

Alonso-Pandavenes, O., Bernal, D., Torrijo, F. J., and Garzón-Roca, J. A Comparative Analysis for Defining the Sliding Surface and Internal Structure in an Active Landslide Using the HVSR Passive Geophysical Technique in Pujilí (Cotopaxi), Ecuador. *Land*, 12 (5):961, Apr. 2023. doi: 10.3390/land12050961.

Bard, P.-Y. and Riepl-Thomas, J. *Wave propagation in complex geological structures and their effects on strong ground motion*, pages 37–95. WIT Press, Southampton, Great Britain, 2000.

Bhattacharyya, K. and Mitra, G. A new kinematic evolutionary model for the growth of a duplex—an example from the Rangit duplex, Sikkim Himalaya, India. *Gondwana Research*, 16(3–4): 697–715, Dec. 2009. doi: 10.1016/j.gr.2009.07.006.

Bhattacharyya, K., Mitra, G., and Kwon, S. Geometry and kinematics of the Darjeeling–Sikkim Himalaya, India: Implications for the evolution of the Himalayan fold-thrust belt. *Journal of Asian Earth Sciences*, 113:778–796, Dec. 2015. doi: 10.1016/j.jseaes.2015.09.008.

Bland, H. and Gallant, E. Avoiding wind noise: How helpful is geophone-burying. *CSEG Geophysics*, pages 1–4, 2002.

Bonamassa, O. and Vidale, J. E. Directional site resonances observed from aftershocks of the 18 October 1989 Loma Prieta earthquake. *Bull. Seismol. Soc. Am.*, 81(5):1945–1957, 1991. doi: 10.1785/BSSA0810051945.

Bonilla, L. F., Steidl, J. H., Lindley, G. T., Tumarkin, A. G., and Archuleta, R. J. Site amplification in the San Fernando Valley, California: variability of site-effect estimation using the S-wave, coda, and H/V methods. *Bulletin of the Seismological Society of America*, 87(3):710–730, June 1997. doi: 10.1785/bssa0870030710.

Bonnefoy-Claudet, S., Cornou, C., Bard, P.-Y., Cotton, F., Moczo, P., Kristek, J., and Fäh, D. H/V ratio: A tool for site effects evaluation. Results from 1-D noise simulations. *Geophysical Journal International*, 167(2):827–837, Nov. 2006. doi: 10.1111/j.1365-246x.2006.03154.x.

Bonnefoy-Claudet, S., Baize, S., Bonilla, L. F., Berge-Thierry, C., Pasten, C., Campos, J., Volant, P., and Verdugo, R. Site effect evaluation in the basin of Santiago de Chile using ambient noise measurements. *Geophysical Journal International*, 176(3): 925–937, Mar. 2009. doi: 10.1111/j.1365-246x.2008.04020.x.

Burjánek, J., Edwards, B., and Fäh, D. Empirical evidence of local seismic effects at sites with pronounced topography: a systematic approach. *Geophysical Journal International*, 197(1): 608–619, Feb. 2014. doi: 10.1093/gji/ggu014.

Burjánek, J., Kleinbrod, U., and Fäh, D. Modeling the seismic response of unstable rock mass with deep compliant fractures. *Journal of Geophysical Research: Solid Earth*, 124(12): 13039–13059, Dec. 2019. doi: 10.1029/2019jb018607.

Chávez-García, F. J., Sánchez, L. R., and Hatzfeld, D. Topographic site effects and HVSR. A comparison between observations and theory. *Bulletin of the Seismological Society of America*, 86(5): 1559–1573, Oct. 1996. doi: 10.1785/bssa0860051559.

Dasgupta, S., Chakraborty, S., and Neogi, S. Petrology of an inverted Barrovian sequence of metapelites in Sikkim Himalaya, India: Constraints on the tectonics of inversion. *American Journal of Science*, 309(1):43–84, Jan. 2009. doi: 10.2475/01.2009.02.

DeCelles, P. G. and Mitra, G. History of the Sevier orogenic wedge in terms of critical taper models, northeast Utah and southwest Wyoming. *Geol. Soc. Am. Bull.*, 107(4):454–462, 1995. doi: 10.1130/0016-7606(1995)107<0454:HOTSOW>2.3.CO;2.

Del Gaudio, V., Coccia, S., Wasowski, J., Gallipoli, M. R., and Mucciarelli, M. Detection of directivity in seismic site response from microtremor spectral analysis. *Natural Hazards and Earth System Sciences*, 8(4):751–762, July 2008. doi: 10.5194/nhess-8-751-2008.

Dietiker, B., Pugin, A. J.-M., Crow, H. L., Mallozzi, S., Brewer, K. D., Cartwright, T. J., and Hunter, J. A. HVSR measurements in complex sedimentary environment and highly structured resonator topography–comparisons with seismic reflection profiles and geophysical borehole logs. In *Symposium on the Application of Geophysics to Engineering and Environmental Problems 2018*, volume 66, page 324–330. Society of Exploration Geophysicists and Environment and Engineering Geophysical Society, Oct. 2018. doi: 10.4133/sageep.31-025.

Field, E. H. and Jacob, K. H. A comparison and test of various site-response estimation techniques, including three that are not reference-site dependent. *Bull. Seismol. Soc. Am.*, 85(4): 1127–1143, 1995.

Formisano, L. A., La Rocca, M., Del Pezzo, E., Galluzzo, D., Fischione, C., and Scarpa, R. Topography effects in the polarization of earthquake signals: a comparison between surface and deep recordings. *Bollettino di Geofisica Teorica ed Applicata*, 53 (4), 2012. doi: 10.4430/bgta0055.

Fäh, D., Kind, F., and Giardini, D. A theoretical investigation of average H/V ratios. *Geophysical Journal International*, 145(2): 535–549, May 2001. doi: 10.1046/j.0956-540x.2001.01406.x.

Galea, P., D'Amico, S., and Farrugia, D. Dynamic characteristics of an active coastal spreading area using ambient noise measurements—Anchor Bay, Malta. *Geophysical Journal International*, 199(2):1166–1175, Sept. 2014. doi: 10.1093/gji/ggu318.

Gautam, P. and Rösler, W. Depositional chronology and fabric of Siwalik Group sediments in central Nepal from magnetostratigraphy and magnetic anisotropy. *Journal of Asian Earth Sciences*, 17(5–6):659–682, Oct. 1999. doi: 10.1016/s1367-9120(99)00021-8.

Geli, L., Bard, P.-Y., and Jullien, B. The effect of topography on earthquake ground motion: A review and new results. *Bulletin of the Seismological Society of America*, 78(1):42–63, Feb. 1988. doi: 10.1785/bssa0780010042.

Gosar, A., Rošer, J., Šket Motnikar, B., and Zupančič, P. Microtremor study of site effects and soil-structure resonance in the city of Ljubljana (central Slovenia). *Bulletin of Earthquake Engineering*, 8(3):571–592, Apr. 2009. doi: 10.1007/s10518-009-9113-x.

Guerriero, L., Revellino, P., Luongo, A., Focareta, M., Grelle, G., and Guadagno, F. M. The Mount Pizzuto Earth flow: Deformational pattern and recent thrusting evolution. *Journal of Maps*, 12(5): 1187–1194, Feb. 2016. doi: 10.1080/17445647.2016.1145150.

Hussain, Y., Martinez-Carvajal, H., Condori, C., Uagoda, R., Cárdenas-Soto, M., Cavalcante, A. L. B., Cunha, L. S. d., and Martino, S. Ambient seismic noise: A continuous source for the dynamic monitoring of landslides. *Terrae Didatica*, 15:e019012, Feb. 2019. doi: 10.20396/td.v15i1.8652455.

Imposa, S., Grassi, S., Fazio, F., Rannisi, G., and Cino, P. Geophysical surveys to study a landslide body (north-eastern Sicily). *Natural Hazards*, 86(S2):327–343, Aug. 2016. doi: 10.1007/s11069-016-2544-1.

Kaur, H., Gupta, S., Parkash, S., Thapa, R., Gupta, A., and Khanal, G. C. Evaluation of landslide susceptibility in a hill city of Sikkim Himalaya with the perspective of hybrid modelling techniques. *Annals of GIS*, 25(2):113–132, Mar. 2019. doi: 10.1080/19475683.2019.1575906.

Kawase, H., Sanchez-Sesma, F. J., and Matsushima, S. The Optimal Use of Horizontal-to-Vertical Spectral Ratios of Earthquake Motions for Velocity Inversions Based on Diffuse-Field Theory for Plane Waves. *Bulletin of the Seismological Society of America*, 101(5):2001–2014, Sept. 2011. doi: 10.1785/0120100263.

Konno, K. and Ohmachi, T. Ground-motion characteristics estimated from spectral ratio between horizontal and vertical components of microtremor. *Bulletin of the Seismological Society of America*, 88(1):228–241, Feb. 1998. doi: 10.1785/bssa0880010228.

La Rocca, M., Chiappetta, G. D., Gervasi, A., and Festa, R. L. Non-stability of the noise HVSR at sites near or on topographic heights. *Geophysical Journal International*, 222(3):2162–2171, June 2020. doi: 10.1093/gji/ggaa297.

Lermo, J. and Chávez-García, F. J. Site effect evaluation using spectral ratios with only one station. *Bulletin of the Seismological Society of America*, 83(5):1574–1594, Oct. 1993. doi: 10.1785/bssa0830051574.

Maresca, R., Guerriero, L., Ruzza, G., Mascellaro, N., Guadagno, F. M., and Revellino, P. Monitoring ambient vibrations in an active landslide: Insights into seasonal material consolidation and resonance directivity. *Journal of Applied Geophysics*, 203: 104705, Aug. 2022. doi: 10.1016/j.jappgeo.2022.104705.

Molnar, S., Cassidy, J. F., Castellaro, S., Cornou, C., Crow, H., Hunter, J. A., Matsushima, S., Sánchez-Sesma, F. J., and Yong, A. Application of microtremor horizontal-to-vertical spectral ratio (MHVSR) analysis for site characterization: State of the art. *Surveys in Geophysics*, 39(4):613–631, Mar. 2018. doi: 10.1007/s10712-018-9464-4.

Molnar, S., Sirohey, A., Assaf, J., Bard, P.-Y., Castellaro, S., Cornou, C., Cox, B., Guillier, B., Hassani, B., Kawase, H., Matsushima, S., Sánchez-Sesma, F. J., and Yong, A. A review of the microtremor horizontal-to-vertical spectral ratio (MHVSR) method. *Journal of Seismology*, 26(4):653–685, Mar. 2022. doi: 10.1007/s10950-021-10062-9.

Moore, J. R., Gischig, V., Burjanek, J., Loew, S., and Fah, D. Site effects in unstable rock slopes: Dynamic behavior of the Randa instability (Switzerland). *Bulletin of the Seismological Society of America*, 101(6):3110–3116, Dec. 2011. doi: 10.1785/0120110127.

Mucciarelli, M., Gallipoli, M. R., Di Giacomo, D., Di Nota, F., and Nino, E. The influence of wind on measurements of seismic noise. *Geophysical Journal International*, 161(2):303–308, May 2005. doi: 10.1111/j.1365-246x.2004.02561.x.

Nakamura, Y. A method for dynamic characteristics estimation of subsurface using microtremor on the ground surface. *Q. Rep. Railw. Tech. Res. Inst.*, 30(1), 1989.

Pal, I., Nath, S. K., Shukla, K., Pal, D. K., Raj, A., Thingbaijam, K. K. S., and Bansal, B. K. Earthquake hazard zonation of Sikkim Himalaya using a GIS platform. *Natural Hazards*, 45(3):333–377, Nov. 2007. doi: 10.1007/s11069-007-9173-7.

Panzera, F., D'Amico, S., Lotteri, A., Galea, P., and Lombardo, G. Seismic site response of unstable steep slope using noise measurements: T he case study of Xemxija Bay area, Malta. *Natural Hazards and Earth System Sciences*, 12(11):3421–3431, Nov. 2012. doi: 10.5194/nhess-12-3421-2012.

Panzera, F., Lombardo, G., Longo, E., Langer, H., Branca, S., Azzaro, R., Cicala, V., and Trimarchi, F. Exploratory seismic site response surveys in a complex geologic area: a case study from Mt. Etna volcano (southern Italy). *Natural Hazards*, 86(S2):385–399, Aug. 2016. doi: 10.1007/s11069-016-2517-4.

Pastén, C., Sáez, M., Ruiz, S., Leyton, F., Salomón, J., and Poli, P. Deep characterization of the Santiago Basin using HVSR and cross-correlation of ambient seismic noise. *Engineering Geology*, 201:57–66, Feb. 2016. doi: 10.1016/j.enggeo.2015.12.021.

Paul, D., McNaughton, N., Chattopadhyay, S., and Ray, K. Geochronology and Geochemistry of the Lingtse Gneiss, Darjeeling-Sikkim Himalaya: Revisited. *J. Geol. Soc. India*, 48 (5):497–506, 1996.

Pavankumar, G. and Manglik, A. Complex tectonic setting and deep crustal seismicity of the Sikkim Himalaya: An electrical resistivity perspective. *Physics and Chemistry of the Earth, Parts A/B/C*, 124:103077, Dec. 2021. doi: 10.1016/j.pce.2021.103077.

Pazzi, V., Tanteri, L., Bicocchi, G., D'Ambrosio, M., Caselli, A., and Fanti, R. H/V measurements as an effective tool for the reliable detection of landslide slip surfaces: Case studies of Castagnola (La Spezia, Italy) and Roccalbegna (Grosseto, Italy). *Physics and Chemistry of the Earth, Parts A/B/C*, 98:136–153, Apr. 2017. doi: 10.1016/j.pce.2016.10.014.

Pilz, M., Parolai, S., Leyton, F., Campos, J., and Zschau, J. A comparison of site response techniques using earthquake data and ambient seismic noise analysis in the large urban areas of Santiago de Chile. *Geophysical Journal International*, 178(2):713–728, Aug. 2009. doi: 10.1111/j.1365-246x.2009.04195.x.

Pischiutta, M., Cultrera, G., Caserta, A., Luzi, L., and Rovelli, A. Topographic effects on the hill of Nocera Umbra, central Italy. *Geophysical Journal International*, 182(2):977–987, June 2010. doi: 10.1111/j.1365-246x.2010.04654.x.

Reiter, L. *Earthquake Hazard Analysis: Issues and Insights*. Columbia University Press, New York, USA, 1990.

Rigo, A., Sokos, E., Lefils, V., and Briole, P. Seasonal variations in amplitudes and resonance frequencies of the HVSR amplification peaks linked to groundwater. *Geophysical Journal International*, 226(1):1–13, Mar. 2021. doi: 10.1093/gji/ggab086.

Rong, M., Fu, L., and Wang, J. On the differences between horizontal-to-vertical spectral ratios caused by earthquakes and ambient noise—A case study of vertical-array observations in Northern China. *Journal of Applied Geophysics*, 182:104171, Nov. 2020. doi: 10.1016/j.jappgeo.2020.104171.

Shapiro, N. M., Campillo, M., Singh, S. K., and Pacheco, J. Seismic channel waves in the accretionary prism of the Middle America Trench. *Geophysical Research Letters*, 25(1):101–104, Jan. 1998. doi: 10.1029/97gl03492.

Singh, A., Kumar, M. R., Pandey, A., and Roy, K. S. Investigation of spatial and temporal variability of site response in the Arunachal Himalaya using ambient seismic noise and earthquake waveforms. *Near Surface Geophysics*, 17(4):427–445, June 2019. doi: 10.1002/nsg.12053.

Singh, A., Kumar, G., Singh, C., Kumar, M. R., Uthaman, M., Saikia, D., and Dubey, A. K. Seismic constraints on the nature and geometry of the downwelling Indian crust beneath Sikkim Himalaya. May 2023. doi: 10.5194/egusphere-egu23-2463.

Sonker, I., Tripathi, J. N., and Swarnim. Landslide susceptibility mapping using morphological and hydrological parameters in Sikkim Himalaya: frequency ratio model and geospatial technologies. *Nat. Hazards*, 120(7):6797–6832, 2024.

Souriau, A., Roulle, A., and Ponsolles, C. Site effects in the city of Lourdes, France, from H/V measurements: implications for seismic-risk evaluation. *Bulletin of the Seismological Society of America*, 97(6):2118–2136, Dec. 2007. doi: 10.1785/0120060224.

Stanko, D., Markušić, S., Strelec, S., and Gazdek, M. HVSR analysis of seismic site effects and soil-structure resonance in Varaždin city (North Croatia). *Soil Dynamics and Earthquake Engineering*, 92:666–677, Jan. 2017. doi: 10.1016/j.soildyn.2016.10.022.

Tiwari, V., Vyghreswara Rao, M., Mishra, D., and Singh, B. Crustal structure across Sikkim, NE Himalaya from new gravity and magnetic data. *Earth and Planetary Science Letters*, 247(1–2): 61–69, July 2006. doi: 10.1016/j.epsl.2006.03.037.

Uthaman, M., Singh, A., Singh, C., Dubey, A., and Kumar, G. Discerning structure and seismic hazards in the Sikkim Himalayas. *Eos*, 102, Mar. 2021. doi: 10.1029/2021eo156044.

Uthaman, M., Singh, C., Singh, A., Jana, N., Dubey, A. K., Sarkar, S., and Tiwari, A. K. Spatial and temporal variation of the ambient noise environment of the Sikkim Himalaya. *Scientific Reports*, 12(1), Jan. 2022. doi: 10.1038/s41598-021-04183-x.

Uthaman, M., Singh, A., Singh, C., Kumar, G., Dutta, A., , Jana, N., and Dubey, A. K. Shear wave velocity and radial anisotropy structure beneath Sikkim Himalaya. In *AGU Fall Meeting Conference Abstracts*, 2023a.

Uthaman, M., Singh, C., Singh, A., Dutta, A., Kumar, G., and Dubey, A. K. Focal Mechanisms and Seismicity of local earthquakes beneath the Sikkim Himalaya. 2023b. doi: 10.57757/IUGG23-2306.

Uthaman, M., Singh, C., Singh, A., Dutta, A., Kumar Dubey, A., and Kumar, G. Seismicity and active tectonics: New insights from Sikkim Himalaya. May 2023c. doi: 10.5194/egusphere-egu23-343.

Uthaman, M., Singh, C., and Singh, A. Characterization of landslide prone zones in Sikkim Himalaya using HVSR. In *ESC General Assembly Abstracts*, 2024a.

Uthaman, M., Singh, C., Singh, A., Hetényi, G., Dutta, A., Kumar, G., and Dubey, A. K. Complex multi-fault dynamics in Sikkim Himalaya: New insights from local earthquake analysis. *Geochemistry, Geophysics, Geosystems*, 25(6), June 2024b. doi: 10.1029/2023gc011363.

Wathelet, M., Chatelain, J.-L., Cornou, C., Giulio, G. D., Guillier, B., Ohrnberger, M., and Savvaidis, A. Geopsy: A user-friendly open-source tool set for ambient vibration processing. *Seismological Research Letters*, 91(3):1878–1889, Apr. 2020. doi: 10.1785/0220190360.

Wesnousky, S. G., Kumar, S., Mohindra, R., and Thakur, V. C. Uplift and convergence along the Himalayan Frontal Thrust of India. *Tectonics*, 18(6):967–976, Dec. 1999. doi: 10.1029/1999tc900026.

Wessel, P., Luis, J. F., Uieda, L., Scharroo, R., Wobbe, F., Smith, W. H. F., and Tian, D. The Generic Mapping Tools Version 6. *Geochemistry, Geophysics, Geosystems*, 20(11):5556–5564, Nov. 2019. doi: 10.1029/2019gc008515.

Withers, M., Aster, R., Young, C., Beiriger, J., Harris, M., Moore, S., and Trujillo, J. A comparison of select trigger algorithms for automated global seismic phase and event detection. *Bulletin of the Seismological Society of America*, 88(1):95–106, Feb. 1998. doi: 10.1785/bssa0880010095.

Yassminh, R., Gallegos, A., Sandvol, E., and Ni, J. Investigation of the regional site response in the Central and Eastern United States. *Bulletin of the Seismological Society of America*, 109(3), Mar. 2019. doi: 10.1785/0120180230.

Ávila Barrientos, L., Yegres-Herrera, L. A., and Flores-Estrella, H. Characterization of landslides in Federal Highway 1D, Baja California, Mexico, using seismic noise records and the HVSR method. *Natural Hazards*, 118(2):1281–1299, June 2023. doi: 10.1007/s11069-023-06053-3.